

Step-scaling with off-shell renormalisation

R. Arthur¹ and P. A. Boyle¹

(RBC and UKQCD Collaborations)

¹*SUPA, School of Physics, The University of Edinburgh, Edinburgh EH9 3JZ, UK*

(Dated: September 6, 2018)

Abstract

We make use of twisted boundary conditions for off-shell, Rome-Southampton renormalisation. This allows us to define vertex functions at a fixed physical momentum that need not be a Fourier mode. This definition includes choosing a fixed orientation with respect to the lattice axes; only then do lattice artefacts, which include $O(4)$ breaking effects, have a valid expansion in powers of the lattice spacing, a . The use of non-exceptional momenta has been found to greatly reduce the dependence of the vertex functions on both mass and momentum, p . Excellent statistical precision is afforded by plane-wave sources. Together this enables both a theoretically well founded and statistically clean continuum limit. Thereafter all p^2 dependence can be identified with the anomalous running of the operator. We present initial results and develop a practical scheme for step-scaling with off-shell renormalization. The size of the steps is continuous rather than discrete, allowing arbitrarily small steps and the scheme is easy to implement for general operators .

I. INTRODUCTION

The non-perturbative renormalisation (NPR) of Lattice QCD matrix elements is an important topic for the phenomenological relevance of the field. This paper addresses two key limitations of the popular Rome-Southampton RI/MOM method[1]: firstly the entangled discretisation and perturbative truncation errors and secondly the rather low scale at which continuum perturbation theory is applied.

Phenomenology requires that scheme dependent QCD observables calculated within lattice QCD are converted to a perturbatively amenable scheme such as \overline{MS} . This is often done using an intermediate, regularisation invariant momentum scheme (known as RI/MOM). The conversion of lattice results to the RI/MOM scheme is non-perturbative and the scale is defined by the momenta used. Obtaining precision in the lattice calculation requires that the momentum scale used is well below the lattice cut-off, giving the high end of the Rome-Southampton momentum “window” condition:

$$\Lambda_{\text{QCD}}^2 \ll p^2 \ll \left(\frac{\pi}{a}\right)^2. \quad (1)$$

The perturbative conversion between RI/MOM (or RI/SMOM in the case of non-exceptional kinematics) and \overline{MS} is known for many operators to as many as three loops. Perturbative accuracy is dependent on satisfying the lower inequality in Eq. (1). The error associated with the low end of the window depends on logarithms the physical momentum scale, while the high end converges more benignly as a power of the dimensionless momentum scale ($(ap)^2$ in the case of domain wall fermions). The continuum extrapolation enabled by this work affords some tolerance to operating near the margins at high momentum by extrapolating away discretisation errors. The step scaling proposed in this work is intended to raise the momentum scale into a more convergent perturbative regime.

The structure of the paper is as follows. In section II we summarise the method of off-shell non-perturbative renormalisation. In section III we introduce twisted boundary conditions for off-shell renormalisation. This is motivated in section III A where we explain how this solves a serious theoretical problem with defining the continuum limit of operators renormalised using RI/MOM. The implementation of twisted boundary conditions in the valence sector for fermion vertex functions is discussed in section III B, and we define lattice kinematics (III C) with which we intend to take the continuum limit (III D) for both ex-

ceptional and non-exceptional momenta. Our proposed step scaling scheme, based on these techniques, is discussed in section IV.

We present data for the amputated vertex functions at a single lattice spacing in section V A. In section V C we demonstrate practicality using existing configurations to take the continuum limit for the first step in the step scaling programme.

II. BACKGROUND

The Rome-Southampton RI/MOM approach [1] involves a simple physically defined momentum scheme, albeit with particularly unphysical renormalisation conditions. For any given operator, \mathcal{O} , a momentum configuration for the vertex function of that operator is chosen with momenta p_μ selected from the Fourier modes for the simulated lattice size aL_μ , where L_μ is an integer:

$$ap_\mu = \frac{2\pi}{L_\mu} n_\mu$$

, with $n_\mu \in \{0, \dots, L_\mu\}$.

The renormalisation condition for any regularization scheme S chooses counter terms such that renormalised amputated vertex function, in Landau gauge and for a chosen set of external momenta, is equal to the tree level operator. For example, for bilinears this is

$$\Lambda_{\mathcal{O}}^{S,ren}(p_1, p_2) = \frac{Z_{\mathcal{O}}^S}{Z_q} \Lambda_{\mathcal{O}}^S(p_1, p_2) = \mathcal{O}^{\text{tree}}, \quad (2)$$

where Λ represents an amputated vertex function. The original paper used the amplitude with

$$p_1 = p_2; q^2 = 0. \quad (3)$$

The approach facilitates the conversion between different schemes because all that is required in any given scheme S is a self-consistent calculation of the relevant scattering amplitude to some order. By virtue of the physical definition, one scheme can be a fully non-perturbative lattice calculation with some lattice action at non-zero lattice spacing. Thus, within the scaling window, Eq (1), a lattice simulation can be matched directly to continuum perturbation theory without use of ill-convergent lattice perturbation theory.

This momentum window argument motivates the neglect of discretisation errors in a certain limit. We shall see in section III that a rigorous continuum extrapolation using the original method is made impossible due to the use of Fourier modes. This is because keeping

both the direction and magnitude of the physical momenta fixed while changing the lattice spacing is incompatible with the discrete momentum spectrum.

A. Non-exceptional momentum

In the original RI/MOM kinematic choice a single gluon can carry all the hard momentum through the vertex leading to infra-red effects which fall only as $\frac{1}{p^2}$. Depending on the operator these effects have a non-trivial dependence on the valence quark mass that can complicate mass extrapolations, and in some cases require pion pole subtraction [1, 5–7].

RBC and UKQCD have developed the non-exceptional momentum, SMOM, kinematic point as a preferred matching condition [8]. A significant gain comes from the extra suppression of non-perturbative effects. The perturbative expansion must be calculated for non-exceptional momenta; this has been performed to one loop for bilinear operators [9] and for B_K [10]. Two recent publications have extended this to two loops for two different schemes for the quark mass [11, 12]. The non-exceptional kinematic point for bilinears has

$$p_1^2 = p_2^2 = (p_1 - p_2)^2. \quad (4)$$

RBC and UKQCD have found [8] that both momentum and mass dependence are simplified with non-exceptional kinematics. With this momentum flow, multiple hard gluons are required to create a soft sub-graph and non-perturbative infra-red effects, such as spontaneous chiral symmetry breaking, fall as a higher power of the external momentum, $\frac{1}{p^6}$ [13]. As our aim is to carefully study vertex functions while reducing the volume, we require a momentum scheme that is not sensitive to condensate physics.

B. Volume source NPR

The original method used a single point source to calculate momentum space Green's functions. The volume source technique was developed by QCDSF [2]. The attraction here is to evaluate the amputated vertex function with the operator insertion averaged over all L^4 lattice sites. We shall see it is easily possible to obtain 0.1% statistical errors with volume source techniques, and even smaller if hundreds of configurations or larger volumes were used. With this statistical precision systematic effects like $\mathcal{O}(4)$ breaking lattice artefacts

are visible and are in fact the dominant systematic error. These must either be included in the error analysis or better yet addressed using the techniques of this paper to escape the Fourier constraints.

We use i, j to represent colour indices, and α, β to represent spin indices. We define the four momentum source, used on a Landau gauge fixed configuration, as

$$\eta_p(x) = e^{ip_\mu x^\mu} \delta_{ij} \delta_{\alpha\beta}, \quad (5)$$

where the (dimensionless) momenta are $ap_\mu = n_\mu \frac{2\pi}{L_\mu}$. On a given gauge field $U_\mu(x)$ we solve

$$\sum_x D_{\text{dwf}}(y, x) G(x, p) = \eta_p(y), \quad (6)$$

and D_{dwf} is the Domain Wall fermion matrix [3]. One propagator inversion for each leg momentum is necessary, but this cost is more than offset by the gain in statistical accuracy from the volume average.

To compute the external legs required for amputating the vertex functions we require the momentum space propagator

$$G(p_1, p_1) = \sum_x e^{-ip_1^\mu x^\mu} G(x, p_1). \quad (7)$$

We form phased propagators for each momentum:

$$G'(x, p) = G(x, p) e^{-ip \cdot x} = \sum_y D_{\text{dwf}}^{-1}(x, y) e^{ip \cdot (y-x)}. \quad (8)$$

We select two independent momenta p_1 , and p_2 , and form unamputated bilinear vertex functions V_Γ for Dirac structure Γ :

$$V_\Gamma^{\text{bilinear}}(p_1, p_2) = \left[\sum_x \gamma_5 (G'(x, p_1))^\dagger \gamma_5 \Gamma G'(x, p_2) \right]_{ij, \alpha\beta}, \quad (9)$$

and also for four quark operators:

$$V_{\Gamma\Gamma}^{\text{4q}}(p_1, p_2) = \sum_x (\gamma_5 (G'(x, p_1))^\dagger \gamma_5 \Gamma G'(x, p_2))_{ij, \alpha\beta} (\gamma_5 (G'(x, p_1))^\dagger \gamma_5 \Gamma G'(x, p_2))_{kl, \gamma\delta}. \quad (10)$$

Here, external colour and spin indices are left free for off line amputation and projection. This allows us to define the amputated Green's function as, for example,

$$\Pi_\Gamma(p) = (G^{-1}(p_1, p_1) V_\Gamma(p_1, p_2) \gamma_5 [G^{-1}(p_2, p_2)]^\dagger \gamma_5) \quad (11)$$

where $p^2 = p_1^2 = p_2^2 = (p_1 - p_2)^2$, and we take $q = p_1 - p_2$. The bare vertex amplitudes are then obtained by projecting the amputated Green's functions onto their tree level values, for example

$$\Lambda_\Gamma = \frac{1}{12} \text{Tr} (\Pi_\Gamma \Gamma). \quad (12)$$

III. CONTROLLED CONTINUUM EXTRAPOLATION

We will motivate and introduce the use of twisted boundary conditions in the context of off-shell renormalisation. This will enable us to develop a framework for better controlled continuum extrapolation than is possible using Fourier modes.

A. Continuum extrapolation and Fourier constraints

In continuum Euclidean space simultaneously rotating all momenta in a scattering amplitude by any $O(4)$ matrix must give equivalent results. However, in our discrete system there is only $H(4)$ symmetry and, even in the infinite volume, only momenta related by $\pi/2$ rotations and reflections are equivalent. Vertex functions will receive *different* $O(a^2)$ errors depending on the direction of the momentum relative to the lattice axes. The original studies did not resolve $\mathcal{O}(4)$ breaking lattice artefacts due to statistical imprecision. Different $\mathcal{O}(4)$ equivalent but $\mathcal{H}(4)$ distinct momentum configurations, given by different Fourier modes, were treated interchangeably and simply averaged together. This is backed to some extent by the Rome-Southampton window argument for a region of safe operation with respect to lattice artefacts.

When the method outlined above is combined with a continuum extrapolation, the naive use of $\mathcal{H}(4)$ inequivalent momenta as interchangeable is theoretically unsound because $O(4)$ breaking is a component of the lattice artefacts that should be removed by the extrapolation. If the orientation of momenta relative to lattice axes does not remain fixed as a is changed, an extrapolation in a is *not* formally valid as one uses a *different* observable for each lattice spacing (differing due to $\mathcal{H}(4)$ inequivalent momentum choices). The Fourier constraints make it difficult to select the same physical momentum simultaneously on more than one lattice spacing, and these differing $O(4)$ breaking lattice artefacts necessarily enter each data point in a continuum extrapolation of data renormalised using the Rome-Southampton

method. This introduces an intrinsic systematic uncertainty at a level set by the size of $O(4)$ breaking artefacts.

$O(4)$ breaking effects were argued to be ignorable as they were not statistically resolved. This justifies smooth interpolation in p^2 to obtain matched physical momenta.

It also somewhat justifies an (otherwise dubious) continuum extrapolation. We measure the vertex function observable on different lattice spacings at the same physical momentum magnitude, but must pick $\mathcal{H}(4)$ inequivalent momenta to satisfy Fourier constraints. This results in incorrectly parametrised lattice artefacts, however $\mathcal{O}(4)$ breaking effects can be safely ignored when they are substantially smaller than statistical errors.

With the volume source technique, however, $O(4)$ breaking effects are well resolved and are a dominant systematic error. This compromises our ability to perform a continuum extrapolation, and these considerations represent a serious problem that we address in this paper with the use of twisted boundary conditions.

B. Twisted boundary conditions

From the discussion of the previous subsection III A we see that it would be rather better to crisply remove lattice artefacts by continuum extrapolation, and only apply perturbative matching in the continuum limit. This is difficult when constrained to use Fourier modes. Applying twisted boundary conditions to propagator inversions enables arbitrary momenta to be used. The twisted boundary approach differs by only finite volume effects from a simulation on a much larger lattice with an exact Fourier mode of the same momentum.

In order to simultaneously satisfy the constraint (4) and only use one momentum direction we propose choosing one kinematic satisfying (4) and use twisted boundary conditions [25–27, 29, 30], to vary the magnitude of the momentum. The twisting technique has been used to insert arbitrary three-momenta in form factor calculations with the success demonstrated, for example, by the direct comparison of refs [31, 32] to refs [30, 33, 34]. which make use of the same configurations and action.

In this paper the technique is used to allow arbitrary four-momenta to be used [25], and hence allow to rigorously disentangle discretisation and perturbative truncation effects for the first time. Of course, the lattice artefacts are still present at finite lattice spacing but, up to finite volume effects, these become the *same* lattice artefact at each lattice spacing. This

is not the case if different Fourier modes are used. The goal is to enable us to determine the non-perturbative anomalous running in the RI scheme in the continuum limit prior to the use of continuum perturbation theory.

We now formulate the momentum space propagator calculation with twisted boundary conditions for use in off-shell renormalisation. Let the quark fields satisfy twisted boundary conditions $q(x + L) = e^{i\theta}q(x)$ and define [28]

$$\tilde{q}(x) = e^{-iBx}q(x) \quad (13)$$

with $aB_\mu = \frac{\theta}{L_\mu}$ so that $\tilde{q}(x)$ satisfies periodic boundary conditions. This transformation changes the continuum Dirac operator:

$$D = (\not{\partial} + m) \rightarrow \tilde{D} = (\not{\partial} + i\not{B} + m) \quad (14)$$

\tilde{D} has inverse \tilde{G} and D has inverse G ; they are related by

$$G(x, y) = e^{iB(x-y)}\tilde{G}(x, y) \quad (15)$$

using translational invariance which we should recover after gauge averaging. Let

$$\tilde{G}(z, p) = \sum_x \tilde{G}(z, x)e^{ipx} \quad (16)$$

then

$$\sum_z \tilde{D}(y, z)\tilde{G}(z, p) = e^{ipy} \quad (17)$$

So inverting the twisted Dirac operator (14) with a momentum source gives $\tilde{G}(z, p)$. Note that $\tilde{G}(z, x)$ satisfies periodic boundary conditions so that in the source term, e^{ipy} , $ap_\mu = \frac{2\pi n_\mu}{L_\mu}$ is a Fourier mode. $\tilde{G}(z, p)$ is related to $G(z, p)$ via,

$$\tilde{G}(z, p) = \sum_x e^{-iB(z-x)}G(z, x)e^{ipx} = e^{-iBz}G(z, p + B). \quad (18)$$

The propagator can be obtained from,

$$\tilde{G}(p, p) = \sum_z e^{-ipz}\tilde{G}(z, p) = \sum_{z,x} e^{-i(p+B)(z-x)}G(z, x) = G(p + B, p + B) \quad (19)$$

Thus the net effect of twisted boundary conditions is to shift the momentum p to $p + B$ where B is arbitrary. In order to compute the non-exceptional Green's functions observe,

$$\tilde{V}_\Gamma(p_1, p_2) = \sum_{x,y,z} e^{-ip_1(x-z)}\tilde{G}(x, z)\Gamma e^{-ip_2(z-y)}\tilde{G}(z, y) = \sum_z \gamma_5 e^{ip_1 z}\tilde{G}(z, p_1)^\dagger \gamma_5 \Gamma e^{-ip_2 z}\tilde{G}(z, p_2) \quad (20)$$

Using the inverse of (18) $\tilde{G}_\Gamma(p_1, p_2)$ the vertex function is seen to be,

$$\tilde{V}_\Gamma(p_1, p_2) = \sum_{x,y} \gamma_5 e^{i(p_1+B_1)x} G(x, p_1+B_1)^\dagger \gamma_5 \Gamma e^{-i(p_2+B_2)y} G(y, p_2+B_2) = V_\Gamma(p_1+B_1, p_2+B_2) \quad (21)$$

We consider the values for p_1 , p_2 , B_1 and B_2 in the following subsection.

C. Kinematics

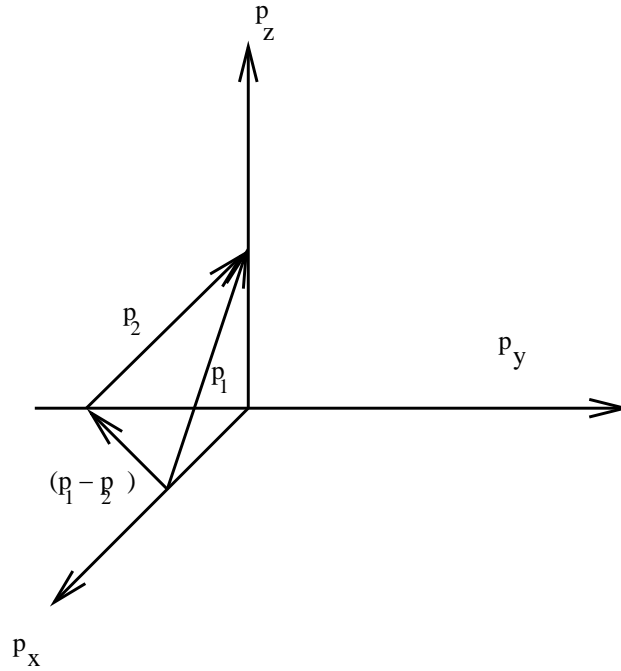


Figure 1: Non-exceptional momentum configuration used in this paper. The momenta p_1 , p_2 and $(p_1 - p_2)$ must be equal in magnitude and are represented as an equilateral triangle with vertices touching the p_x , p_y , and p_z axes. With twisted boundary conditions the sides of this triangle can be continuously scaled allowing both smooth interpolation of momentum dependence and controlled continuum extrapolation. This is very much in contrast to the situation that arises when using only Fourier modes.

We select Euclidean momenta in the direction of $p_1 = (-1, 0, 1, 0)$ and $p_2 = (0, 1, 1, 0)$ up to $H(4)$ symmetry operations. This choice minimises $S^4 = \sum_i p_i^4$ which we take as measure of discretization errors, subject to the constraint that $p_1/p_2/(p_1 - p_2)$ be $H(4)$ equivalent momenta. It is certainly possible to rotate some combination of p_x, p_y, p_z into the temporal

direction breaking this $H(4)$ equivalence, and this would form an interesting possibility to demonstrate universality of the continuum limit in a later work.

The non-exceptional $p_1/p_2/(p_1 - p_2)$ kinematics can be represented by an equilateral triangle in momentum space with vertices lying on the p_x, p_y, p_z coordinate axes (figure 1). Continuous dilation of this triangle can be performed by using twisted boundary conditions with a fixed orientation of the $p_1, p_2, p_1 - p_2$ triangle. This continuity allows one to pick a fixed MOM observable as the lattice spacing is varied. In particular, we choose parallel twisting vectors in the directions $B_1 = (-\theta, 0, \theta, 0)$ corresponding to p_1 and $B_2 = (0, \theta, \theta, 0)$ corresponding to p_2 . We continuously vary θ to move the vertices of the triangle along the axes.

The non-exceptional momenta are chosen to have small discretisation errors by spreading the power across multiple coordinate axes. In general for any non-exceptional configuration there will be $O(a^2)$ errors. For exceptional momentum amplitudes we take vertex functions with p_1 on both legs. As the direction is kept fixed the vertex function is a smooth function of $(ap)^2$ and interpolation in momentum is possible. Extrapolation to the continuum limit at fixed physical momentum is now theoretically justified.

D. Continuum extrapolation

Between different lattice spacings we compare only renormalised quantities and their ratios. This is quite natural as we desire to take the continuum limit of the product of a bare operator matrix element and its RI scheme renormalisation constant at some accessible scale p . The scaling factors for each operator to match between different β 's introduced in [23] are then not required. The aim of the latter part of this paper will be to raise, in the continuum limit, this scale p to one ($s^n p$ where s is a scale factor) where there is better perturbative convergence.

We eliminate Z_q via the vertex function of the (conserved) vector or axial currents:

$$R_{\mathcal{O}}(p, a, m) = \frac{\Lambda_A(p, a, m)}{\Lambda_{\mathcal{O}}(p, a, m)} = \frac{Z_{\mathcal{O}}(p, a, m)}{Z_A} \quad (22)$$

and this ratio will be extrapolated to the chiral limit to produce a renormalization constant

$$Z_{\mathcal{O}}(a, p) = Z_A \lim_{m \rightarrow 0} R_{\mathcal{O}}(p, a, m) \quad (23)$$

where, for convenience, we use the vertex function of the local rather than conserved axial current and eliminate this with a previously computed Z_A . We then continuum extrapolate the product of $Z_{\mathcal{O}}$ with $\langle \mathcal{O} \rangle$:

$$\langle \mathcal{O} \rangle^{\text{ren}} = \lim_{a \rightarrow 0} \langle \mathcal{O} \rangle Z_{\mathcal{O}}. \quad (24)$$

This gives $\langle \mathcal{O} \rangle$ in the RI/MOM scheme at a scale determined by the physical momentum chosen which must be the same scale on all the lattices used to take the continuum limit.

We also consider the factor required to convert $\langle \mathcal{O} \rangle$ at scale p to scale sp where $s > 1$ is a scale factor. This is

$$\Sigma_{\mathcal{O}}(p, sp, a) = \lim_{m \rightarrow 0} \frac{R_{\mathcal{O}}(sp, a, m)}{R_{\mathcal{O}}(p, a, m)}, \quad (25)$$

and its continuum limit is

$$\sigma_{\mathcal{O}}(p, sp) = \lim_{a \rightarrow 0} \Sigma_{\mathcal{O}}(p, sp, a). \quad (26)$$

$\sigma_{\mathcal{O}}(p, sp)$ encodes the scale dependence of the RI scheme in the continuum limit expanded around the scale p . We can then assess the degree to which the running around our match scale is perturbative without risk of confusion by possible lattice artefacts. By picking a well defined momentum orientation for the amplitude as a function of a , we remove the ambiguity in taking the continuum limit that arises when selecting different Fourier modes for each value of β .

We have demonstrated how to obtain a controlled expansion in powers of the lattice spacing for amputated vertex functions and gain better control of lattice artefacts via continuum extrapolation.

IV. STEP SCALING

QCD perturbation theory at lattice scales is not rapidly convergent, and a means to increase this scale without applying brute force to raise the lattice cut-off is required. Step-scaling [14, 15] is the natural approach to do this where, in a series of simulations, the physical volume is reduced as the lattice spacing is reduced to enable the renormalisation scale to be raised without the cost associated with simulating all scales on a single lattice.

A. Step scaling background

Step scaling has been well developed in the Schrödinger functional approach [14–16, 16–20]. A finite volume scheme based on Creutz ratios has also been recently developed [21]. In this paper we seek to develop a related approach based on the Landau gauge fixed RI/MOM method. Our approach does not tie the renormalisation scale to the volume, and therefore also avoids the need to fine tune bare couplings to precisely match a volume sensitive renormalised coupling between simulations.

After reviewing existing step scaling methods we will attempt to address perturbative errors associated with the low-end of the Rome-Southampton scaling window by raising the scale at which we match to perturbation theory by introducing a new step scaling scheme. In order to use the same notational conventions as the literature on step scaling in the Schrödinger functional scheme, for the rest of this section let L represent the length of the lattice in physical units rather than units of lattice spacing. This departs from our convention elsewhere in the paper, which takes L as an integer lattice size and is consistent with notation typically used for RI/MOM renormalization.

1. Schrödinger functional

In step scaling there is typically a renormalisation condition imposed that is physically defined in a fictional finite volume universe. In the case of the Schrödinger functional this is the coupling $\bar{g}(\mu)$ at a scale $\mu = \frac{1}{L}$ defined by the volume. A second simulation, at the same bare coupling and with larger volume sL , then gives the coupling at a scale $\mu' = \frac{\mu}{s} = \frac{1}{sL}$

$$\bar{g}(\mu', a) = \Sigma(s, \bar{g}(\frac{1}{L}), \frac{a}{L}).$$

Here $s > 1$ is a scale factor, and is typically $s = 2$. The continuum limit

$$\sigma(s, \bar{g}(\frac{1}{L})) = \lim_{a \rightarrow 0} \Sigma(s, \bar{g}(\frac{1}{L}), \frac{a}{L}) = \lim_{a \rightarrow 0} \bar{g}(\mu' = \frac{1}{sL}, a),$$

is taken *while holding the measured coupling $\bar{g}(\mu = \frac{1}{L})$ fixed*. Hence $\bar{g}(\mu = \frac{1}{L})$ has no a dependence and the trajectory to the continuum limit leaves the renormalised coupling $\bar{g}(\mu = \frac{1}{L})$ lattice artefact free at (and only at) the scale $\mu = \frac{1}{L}$.

However, $\bar{g}(\mu', a)$ is lattice spacing dependent, with discretisation errors that are removed by taking this continuum limit. Thus $\bar{g}(\mu = \frac{1}{L})$ is the observable quantity used to define

the lattice spacing and hence physical volume. The Schrödinger functional is particularly economical since this is in fact the most infra-red scale accessible within the simulated volume.

When two consecutive scale evolution steps are considered, two sequences of simulations must be performed to determine the evolution of the coupling from scale $\mu'_1 \rightarrow \mu_1$, and from $\mu'_2 \rightarrow \mu_2$ in such a way that $\mu_2 = \mu'_1$. Since *different quantities* $\bar{g}(\mu_1)$ and $\bar{g}(\mu_2)$ are held fixed for the two sequences of simulations (and effectively determine the lattice spacings), satisfaction of the constraint $\mu_2 = \mu'_1$ in the continuum limit is ensured by defining the scaling trajectory for the second sequence such that $\bar{g}(\mu_2, a) = \bar{g}(\mu'_1, a \rightarrow 0)$.

Since each simulation must correctly describe the length scales associated with the quantity used to determine trajectory to the continuum limit, carefully changing this between steps was a key component allowing the volume to be reduced. This is a feature we intend to reproduce in our method.

In the Schrödinger functional $\bar{g}(\frac{1}{L})$ defines the scaling trajectory and is *directly* coupled to the volume. Taking the continuum limit holding $\bar{g}(\frac{1}{L})$ fixed then requires fine tuning of β to *exactly* match the desired non-perturbative coupling – and hence to match physical volumes defined by using $\bar{g}(\frac{1}{L})$ to set the scale. This is a fine tuning step that our proposal below avoids.

2. Previous work on step scaling RI/MOM

The possibility of step scaling with RI/MOM has been previously studied [22], [23]. This work used a series of quenched configurations where the ratio of lattice spacings had been tuned to be precisely a factor of two to obtain aligned Fourier modes. This fine tuning is expensive in a dynamical simulation. Use of power counting and the Rome-Southampton scaling window was made, rather than the controlled continuum extrapolation at fixed physical momentum introduced in this paper. Free parameters for each operator were introduced to match the renormalisation constants for different β 's corresponding to the (possibly non-perturbative) anomalous scaling of the operator with the lattice cut-off. This excellent start was not easily developed into a practical technique.

B. RI/MOM Step Scaling Proposal

In order to develop a practical step scaling scheme we require several pieces. Firstly, we have defined continuum limit non-perturbative evolution ratios that can be used to access higher momentum scales. Step scaling will combine a sequence of these objects, each determined inexpensively compared with a brute force method.

We believe that three technical advantages we have over the earlier attempt at RI/MOM step scaling make the task more tractable. The first, volume sources, reduces statistical errors greatly giving precision to the approach. The second, non-exceptional momenta, renders mass dependence and infra-red behaviour in p^2 benign; this greatly assists with both chiral extrapolation and matching between ensembles, in addition to finite volume sensitivity. These were described above.

In this paper we have introduced a third advantage: using twisted boundary conditions to select arbitrary four momenta. The direction of the scattering momenta can be kept fixed relative to lattice axes and arbitrary values of p^2 can be chosen. This is a Good Thing because it allows the same physical momenta according to the lattice symmetries $H(4)$ to be chosen on each ensemble. The vertex function observable will *only then* have a valid expansion in powers of the lattice spacing a . This approach enables precise matching of momenta between ensembles, and precise continuum extrapolation.

We will keep the off-shell momentum scales hard enough that the physical volume should not be resolved. In this way the calculation will be finite volume effect safe, and the perturbative matching will use the standard infinite volume perturbation theory already available to high order for off-shell renormalisation. These are significant advantages over the Schrödinger functional.

For the scheme to be affordable it is therefore necessary that it be able to operate in a small physical volume. For offshell amplitudes this is the case whenever the virtuality is too hard to resolve the finite volume

$$p^2 \gg \left(\frac{\pi}{L}\right)^2. \quad (27)$$

Thus, for the purposes of step scaling, the window condition Eq (1) becomes

$$\left(\frac{\pi}{L}\right)^2 \ll p^2 \ll \left(\frac{\pi}{a}\right)^2. \quad (28)$$

This latter condition is likely possible to meet using modest lattice volumes $\frac{L}{a} \leq 16$ at all

stages of the calculation. We will compute vertex functions on lattices at different values of β with overlapping scaling windows. This will then enable the determination of a continuum step scaling function for some operator \mathcal{O} at a physical scale p^2 chosen in the window Eq (28) to that at a scale larger by a scale factor s . This is precisely $\sigma_{\mathcal{O}}(p, sp)$ from the previous section.

These can be combined in a series of non-perturbative steps to a high scale, with perturbative conversion to \overline{MS} is then applied only where it is well convergent. For example,

$$\begin{aligned}
\langle \mathcal{O}^{\overline{MS}}(\mu) \rangle &= \langle \mathcal{O}^{\text{SMOM}}(p) \rangle \\
&\times \sigma_{\mathcal{O}}^1(p, sp) \\
&\times \sigma_{\mathcal{O}}^2(sp, s^2p) \\
&\dots \\
&\times \sigma_{\mathcal{O}}^n(s^{n-1}p, s^n p) \\
&\times \left[1 + c^{\text{SMOM} \rightarrow \overline{MS}} \alpha_s(\mu = s^n p) \right].
\end{aligned} \tag{29}$$

It appears clear that Eq (28) can be satisfied at reasonable expense. For example 16^3 domain wall fermion simulations will be inexpensive with the next generation of supercomputers; multiple such ensembles dedicated solely to the renormalisation of lattice operators are quite affordable. This is particularly helped by the relatively benign mass dependence of non-exceptional momentum vertex functions. It is also clear that on these proposed small ensembles all hadronic quantities must be avoided to ensure finite volume safety of the analysis. For the determination of m_{res} , the PCAC is an operator relation and so it is immaterial whether a finite volume or a physical pion state is used to determine the ratio. Determining the lattice spacing (or more specifically the ratio of the lattice spacing to that of an earlier larger volume simulation) in a finite volume safe manner is discussed below.

1. Trajectory to continuum limit

We now define how the continuum limit of $\Sigma_{\mathcal{O}}^n(s^{n-1}p, s^n p, a)$ should be taken to obtain $\sigma_{\mathcal{O}}^n(s^{n-1}p, s^n p)$. In order to avoid the fine tuning problem we seek a quantity q associated with a continuously variable length scale L_q significantly shorter than the lattice extent L to determine the trajectory to the continuum limit. We plan to reduce the volume successively with each step, and a different definition of the lattice spacing (e.g. a different L_q) must be used for each step.

In the Schrödinger functional method this is done by fine tuning (i.e. constraining) $\bar{g}(\mu_{n+1})$ for each non-zero lattice spacing entering the continuum extrapolation of σ^{n+1} to match the continuum limit of the high scale coupling obtained from the previous step, $\lim_{a \rightarrow 0} \bar{g}(\mu'_n, a)$. We seek a family of scale determining quantities $\{q_n\}$ that each be used to determine the lattice spacing in the corresponding n -th step of the step scaling scheme. These will play part of the role that $\bar{g}(\mu = \frac{1}{L})$ plays for the Schrödinger functional.

The continuum limit of successive quantities q_n in the sequence will be determined non-perturbatively as we proceed. Previously determined values will be used to define the trajectory to the continuum limit for successive steps. As a concrete example our initial results we will take q_n to be the static inter-quark force and so the determination of the lattice spacings corresponds to a family of Sommer scales based on the static potential. In the Schrödinger functional the quantity q_n corresponds to the coupling $\bar{g}(\frac{1}{s^n L})$.

At step n we will determine the continuum limit of q_{n+1} while determining the lattice spacing $a^{(q_n)}$ from q_n , and thus must maintain the constraint $q_n(a) = q_n^{\text{cont}}$ while taking the continuum limit:

$$q_{n+1}^{\text{cont}} = \lim_{a^{(q_n)} \rightarrow 0} q_{n+1}(a^{(q_n)}) \Big|_{q_n(a) = q_n^{\text{cont}}} , \quad (30)$$

so that, for example, we determine the continuum limit of the inter-quark force at a reduced length scale in one step, and then reuse this to constrain the trajectory to the continuum limit in the next step. Using this trajectory we define the scale evolution functions σ^n ,

$$\sigma_{\mathcal{O}}^n(s^{n-1}p, s^n p) = \lim_{a^{(q_n)} \rightarrow 0} \Sigma_{\mathcal{O}}^n(s^{n-1}p, s^n p, a^{(q_n)}) \Big|_{q_n(a) = q_n^{\text{cont}}} , \quad (31)$$

where q_n^{cont} is determined by the previous step.

When q is a function of a continuous scale $L_q \ll L$, this distance can be varied post simulation and without finite volume effects, and this allows us to avoid fine tuning β . Ultimately this process will become difficult as all dependence on lattice spacing becomes logarithmic and precision quantities are required; however, there may also be less appropriate but expedient choices that enable immediate progress for a few steps away from our relatively coarse simulations. We consider two possibilities.

Static potential

We note the static potential has been measured successfully over a large range of length scales in the quenched approximation with the Wilson gauge action [35]. This involved the use of a shorter length scale $r_c \simeq 0.26\text{fm}$ than the more common $r_0 \simeq 0.48\text{fm}$ [36]. This calculation is also interesting because it successfully fits $\log \frac{a}{r_0}$ as a polynomial in β . Such an approach may ultimately assist continuing lattice spacing determinations to increasingly fine and small volume simulations.

We consider a sequence of scales, of the same class as the Sommer scale

$$r_n^2 F(r_n) = C_n. \quad (32)$$

The Sommer scale r_0 takes

$$C_0 = 1.65 \quad (33)$$

Thus a step scaling scheme with scale factor s can then be defined choosing $p_n = s^n p$ and $r_n = \frac{r_0}{s^n}$ as follows:

- Determine $\sigma(p_0, p_1)$ in continuum limit holding $r_0 p_0$ fixed such that $r_0^2 F(r_0) = C_0$
 - Determine $C_1 = \frac{r_0^2}{s^2} F(\frac{r_0}{s})$ in continuum limit holding r_0 fixed
 - Decrease L by $\simeq \frac{1}{s}$ without fine tuning
 - Determine $\sigma(p_1, p_2)$ in continuum limit holding $r_1 p_1$ fixed such that $r_1^2 F(r_1) = C_1$
 - Determine $C_2 = \frac{r_1^2}{s^2} F(\frac{r_1}{s})$ in continuum limit holding r_1 fixed
 - Decrease L by $\simeq \frac{1}{s}$ without fine tuning
- etc...

Following a rule of thumb that $r < \frac{L}{3}$ for the static potential should ensure finite volume safety and enable simulation down to $L \simeq 0.75\text{fm}$ when using scales similar to r_c to set the scale. Eventually this will become imprecise when entering a region where the potential runs logarithmically. However we believe a substantial benefit is already achievable prior to addressing this issue.

Alternative schemes

In principle, we can use the momentum dependence of the off-shell vertex functions themselves to match the lattice scales between different ensembles. This may be assisted by the improved techniques of this paper, particularly the tunable momentum scale which allows us to select the length scale that sets lattice spacing. This will be the subject of further study.

If we accept fine tuning, it is also possible to combine step scaling of off-shell vertex functions with existing finite volume schemes such as the Schrödinger functional or the Wilson loop scheme used to match lattice spacings.

V. RESULTS

We use the domain wall fermion action [3], and $16^3 \times 32$ ensembles with $L_s = 16$ and with the Iwasaki gauge action [4]. We use two ensemble sets in this paper, with $\beta = 2.13$ and $\beta = 2.23$. The $\beta = 2.13$ ensembles were studied extensively in Ref. [37]. The three $\beta = 2.13$ 16^3 ensembles used in this section have strange quark mass $m_h = 0.04$ and degenerate light quark masses $m_l = 0.01, 0.02, 0.03$. The second ensemble set with $\beta = 2.23$ is not previously published and was used as part of a parameter search, made in the style of [38, 39], prior to our 32^3 simulations [40] which lie nearby in parameter space. There are two ensembles with $m_h = 0.04$ and $m_l = 0.01, 0.02$. There are around 2000 trajectories in these ensembles.

For $\beta = 2.13$ the extrapolations to $m_q = -m_{res}$ were made with $m_{res} = 0.00305$, $Z_A = 0.7161(1)$, and the lattice spacing was taken as $a^{-1} = 1.729$ GeV [41]. We find in this paper that $\beta = 2.23$ corresponds to an inverse lattice spacing of around $a^{-1} \simeq 2.14$ GeV, we estimate $m_{res} \simeq 10^{-3}$ and $Z_A = 0.740$ by interpolating between nearby values for β . This is not ideal, but adequate for the purposes of this demonstration.

All of the vertex function data was computed using the volume source method with twisted boundary conditions as described in section III B using 20 gauge configurations for each mass, see tables I and II with momenta in table III.

am_q	Range	Δ
0.03	800 - 2320	80
0.02	1000 - 2520	80
0.01	1000 - 2520	80

Table I: $\beta = 2.13$ lattice giving the range of molecular dynamics time and the separation Δ between gauge configurations used in this work. Because so few configurations are needed with the volume averaging a large Δ was chosen to minimise auto-correlation effects.

am_q	Range	Δ
0.02	1000 - 1760	40
0.01	1240 - 2000	40

Table II: $\beta = 2.23$ lattice giving the range of molecular dynamics time and the separation Δ between gauge configurations used in this work.

A. Vertex functions with twisted boundary conditions at a single lattice spacing

In this section we focus on the data obtained using the $\beta = 2.13$ ensembles and display the quality of data obtained on a single lattice spacing.

Figure 2 contains a comparison of the traditional volume averaged Fourier mode NPR to our new twisted boundary condition technique. We show the vector and axial vertex functions at fixed quark mass, $m_q = 0.03$, and with exceptional momentum kinematics on the $\beta = 2.13$ lattice, using 10 configurations. $O(4)$ breaking lattice artefacts produce a large

β	ap_1	ap_2	Range
2.13	$(0, x, x, 0)$	$(-x, 0, x, 0)$	$x = \frac{2\pi}{L}(1.875) \rightarrow x = \frac{2\pi}{L}(2.75)$
2.23	$(0, x, x, 0)$	$(-x, 0, x, 0)$	$x = \frac{2\pi}{L}(1.5625) \rightarrow x = \frac{2\pi}{L}(3.125)$

Table III: The momenta at which we calculated the vertex functions. We note that the momentum $\frac{2\pi}{L}(0, 1.875, 1.875, 0)$, for example, can be reached using 'base' momentum $\frac{2\pi}{L}(0, 1, 1, 0)$ and twist $\frac{2\pi}{L}(0, 0.875, 0.875, 0)$ or base $\frac{2\pi}{L}(0, 2, 2, 0)$ and twist $\frac{2\pi}{L}(0, -0.125, -0.125, 0)$. We chose the base momentum such that the magnitude of the twisting component was less than $\frac{2\pi}{L}(0.75)$, but such a choice is entirely arbitrary.

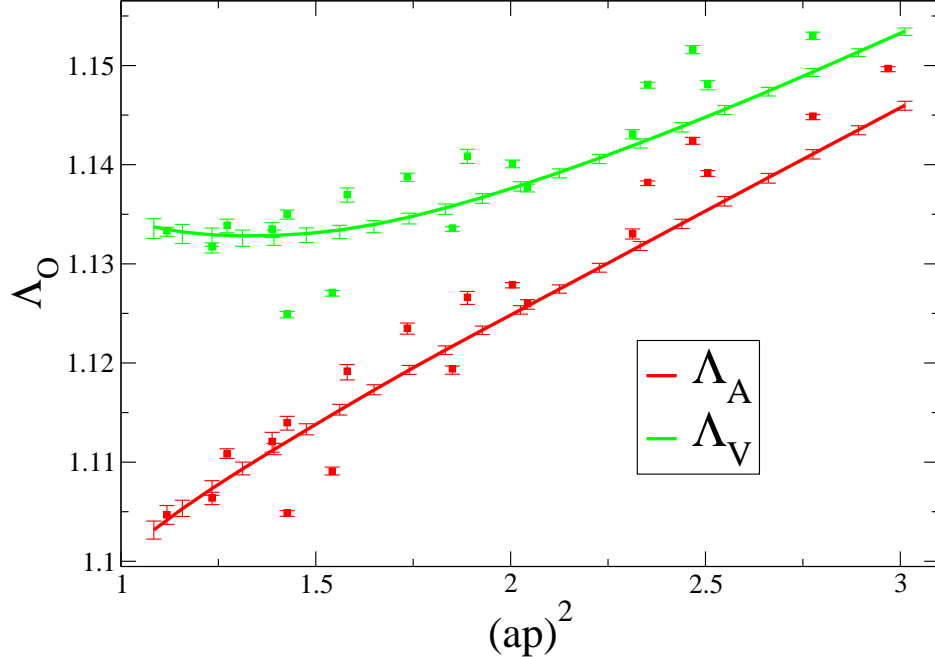


Figure 2: The axial (red) and vector (green) vertex functions on the $\beta = 2.13$ lattice at $m_q = 0.03$, see Section V A for more details. Comparing untwisted (squares) with twisted (connected) data; twisting completely eliminates the $O(4)$ breaking scatter.

scatter in the data using the traditional approach and this is scatter completely removed by the twisted boundary conditions technique. Of course, lattice artefacts are still present and of the same size, but the key point is that we can now vary β while looking at the same off-shell momentum in order to extrapolate these away in the continuum limit.

For the exceptional kinematic configuration we use the projectors of [8] and the perturbative running and matching calculated in [42] for mass and [43] for the tensor current. For \mathcal{O}_{VV+AA} we use the results of [44, 45]. We denote these exceptional momentum schemes RIMOM.

For non-exceptional kinematics we compare the two schemes introduced in [9]. The first is the scheme of [9] which corresponds to choosing projectors $\not{q}q_\mu$ for the vector vertex function and $\not{q}q_\mu\gamma_5$ for the axial vertex function. We denote this scheme SMOM- q . The second uses γ_μ and $\gamma_\mu\gamma_5$ for vector and axial vertex functions, we refer to this scheme as SMOM- γ_μ . The one-loop matching and two-loop anomalous dimensions for tensor current and mass are given in [9]. These results have recently been extended to two loop matching and three

loop anomalous dimensions [11, 12]. For \mathcal{O}_{VV+AA} we use several unpublished new schemes and perturbative results by Sachrajda and Sturm [10], and we thank them for their private communications.

Figure 3 displays the vertex functions of all the operators analysed in this paper (bilinear Vector, Axial Vector, Scalar, Pseudoscalar, Tensor and four quark operator \mathcal{O}_{VV+AA}) for the $\beta = 2.13$ ensemble, for both non-exceptional and exceptional momenta. We will return study each of these structures in turn and in more detail below.

We wish to eliminate the wavefunction renormalisation by taking ratios $\frac{\Lambda_A}{\Lambda_O}$ and where Λ_A is the vertex function of the local axial current, and its renormalisation is eliminated using Z_A previously determined from the ratio of matrix elements the local axial current and the conserved axial current. From the Ward identities in the limit of small mass and large momentum we should find that $Z_V \simeq Z_A$ and $Z_S = Z_P$. These are well supported by our data for non-exceptional momentum but, over our momentum range, not held for exceptional momentum. In order to compare with previous results we adopt, for exceptional momentum, the the strategy of [8] eliminating the quark field renormalisation using

$$\frac{Z_q}{Z_A} = \frac{1}{2}(\Lambda_A + \Lambda_V), \quad (34)$$

where factors of Z_A are then multiplied out using a previously calculated value. For exceptional data this matches central value conventions with [8]. The 2% difference between $\frac{1}{2}(\Lambda_A + \Lambda_V)$ and Λ_A is a chiral symmetry breaking uncertainty that propagates globally in operator renormalisation analysis as a systematic uncertainty (and is doubled for four quark operators). This uncertainty is eliminated for the non-exceptional momentum kinematic 4.

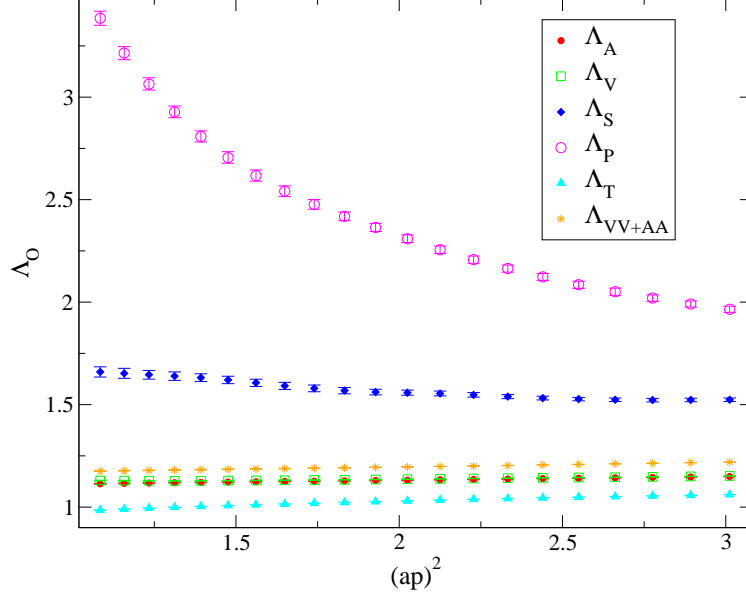
For the non-exceptional case we use simply $\frac{Z_q}{Z_A} = \Lambda_A$. In this case, we have

$$Z_m Z_A = \frac{\Lambda_S}{\Lambda_A}, \quad (35)$$

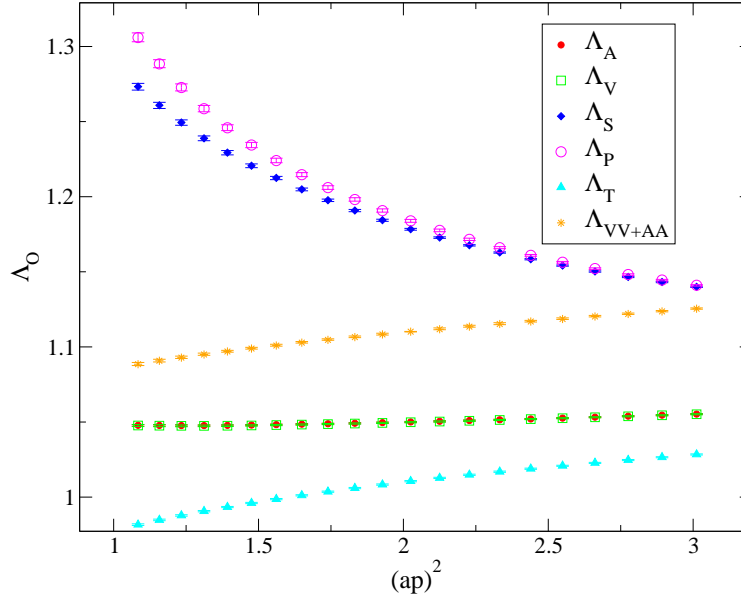
$$\frac{Z_T}{Z_A} = \frac{\Lambda_A}{\Lambda_T}, \quad (36)$$

$$Z_{B_K} = \frac{Z_{\mathcal{O}_{VV+AA}}}{Z_A^2} = \frac{\Lambda_A^2}{\Lambda_{\mathcal{O}_{VV+AA}}}. \quad (37)$$

Our results for RIMOM, SMOM- q , and SMOM- γ_μ schemes for the wave function renormalisation determined from the axial current vertex function (non-exceptional) and average of axial and vector vertex functions (exceptional) are displayed in figure 5. Here, the running at this lattice spacing is poorly described by continuum perturbation theory, and is associated with the momentum dependence of the exponent for binding of light modes in the

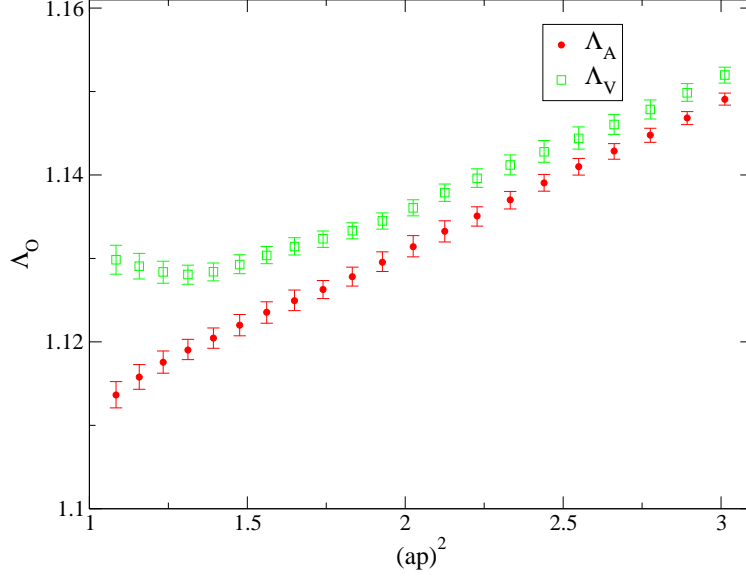


(a) Λ_O exceptional

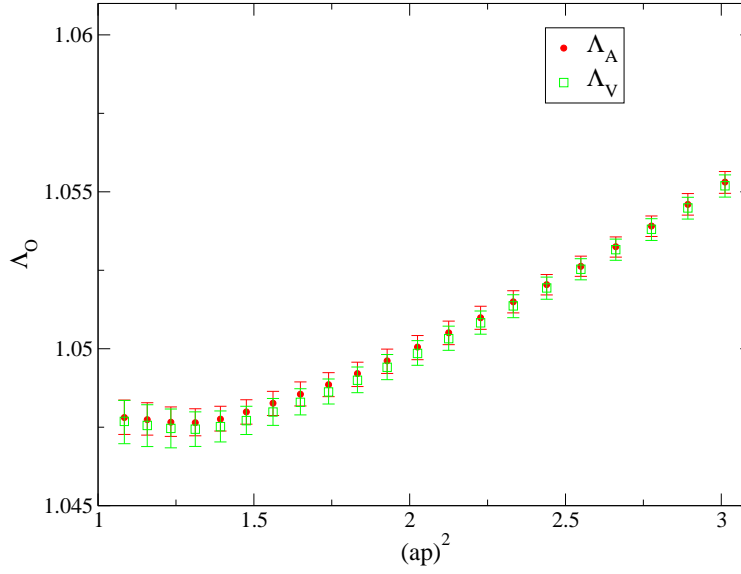


(b) Λ_O non-exceptional γ_μ scheme

Figure 3: All the vertex functions that have been calculated on the $\beta = 2.13$ lattice. Non-exceptional and exceptional vertex functions in the chiral limit. Note the great reduction in chiral symmetry breaking effects ($\Lambda_A - \Lambda_V$ and $\Lambda_S - \Lambda_P$) at non-exceptional momentum.

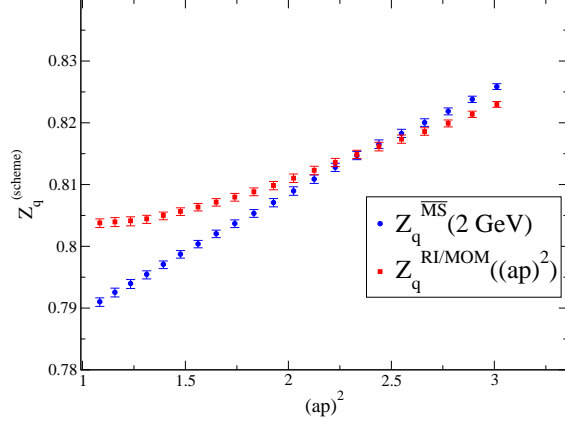


(a) Λ_A, Λ_V exceptional

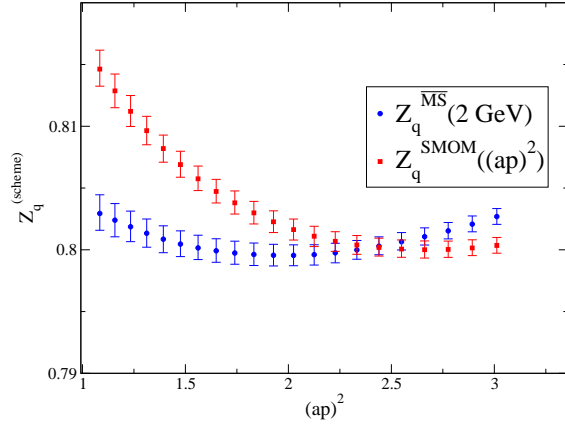


(b) Λ_A, Λ_V non-exceptional γ_μ scheme

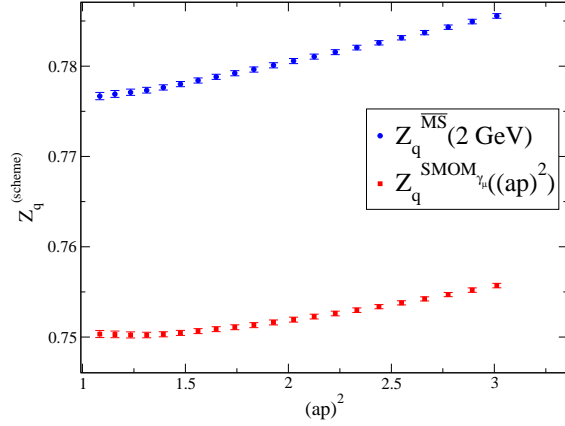
Figure 4: Zoomed in view of Λ_A and Λ_V in the chiral limit with non-exceptional and exceptional kinematics from figure 3. Note the expanded scale in the non-exceptional plot. The roughly 2% difference in the exceptional case is eliminated, even at the lowest momenta, for non-exceptional kinematics.



(a) $Z_q^{RI/MOM}((ap)^2) \rightarrow Z_q^{\overline{MS}}(2\text{GeV})$



(b) $Z_q^{SMOM-\not{d}}((ap)^2) \rightarrow Z_q^{\overline{MS}}(2\text{GeV})$



(c) $Z_q^{SMOM-\gamma\mu}((ap)^2) \rightarrow Z_q^{\overline{MS}}(2\text{GeV})$

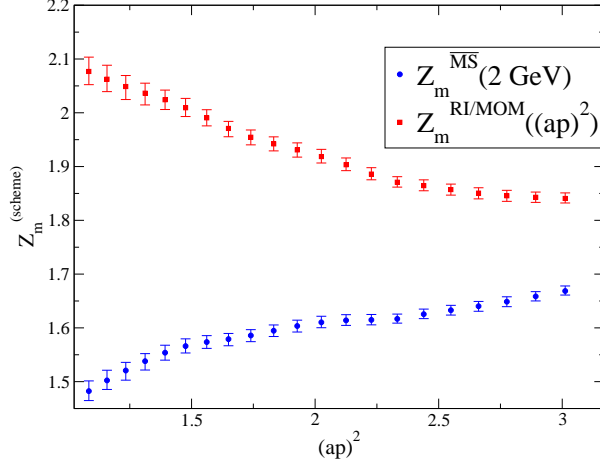
Figure 5: Z_q on the $\beta = 2.13$ lattice in a MOM scheme (red) and with the perturbative running divided out and converted to \overline{MS} (blue). Z_q contains strong lattice artefacts for DWF and is opposite to the continuum running. We find later that this becomes consistent in the continuum limit.

fifth dimension in the domain wall formulation [46]. We note that this Z_q is cancelled in the ratios above when treating other operators. Naturally, one expects that such discretisation effects will be removed if a controlled continuum limit is taken, and this will be revisited in later sections.

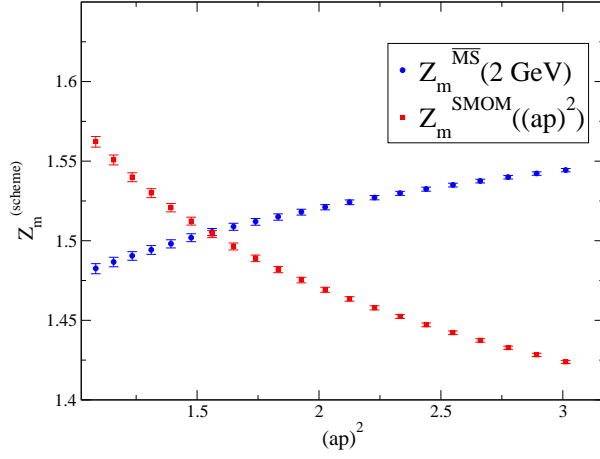
Figures 6, 7, and 8 display the corresponding data for the mass, tensor current and four quark operator \mathcal{O}_{VV+AA} relevant for B_K . As promised, the data is extremely precise and $\mathcal{O}(4)$ breaking discretisation effects do not introduce scatter in the data as the momentum is changed because we are always selecting the same lattice momentum with our twisted boundary conditions. Errors are at the 0.1% level even on this relatively small volume and with only twenty configurations.

In contrast to Z_q , the running of Z_m , Z_T , and Z_{VV+AA} is reasonably well described by continuum perturbation theory for larger values of p^2 , even on this non-zero lattice spacing. This is indicated by reduction of the slope of the data after perturbative conversion to \overline{MS} (blue) especially at higher momenta. Residual p^2 dependence remains after this conversion at the few percent scale. This reflects an admixture of lattice artefacts, and perturbative truncation error. The methods introduced in this paper enable the continuum limit of the scale evolution to be determined and disentangle these sources of error.

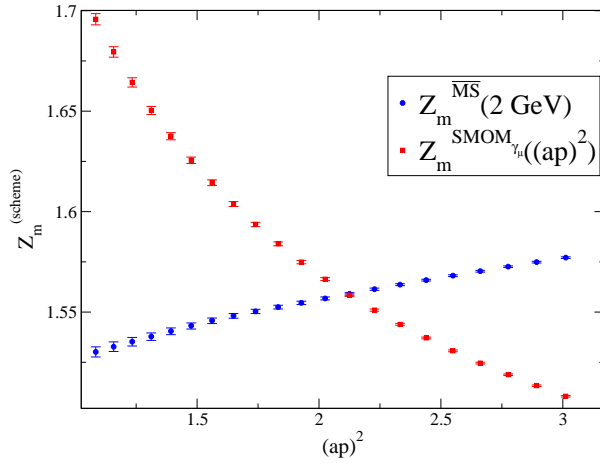
Table IV shows our results compared with the results of Ref [8] after following the same procedure of converting to the \overline{MS} scheme at 2 GeV and then extrapolating to $p^2 = 0$. In all cases the extrapolation was performed using a linear fit of Λ_O as a function of $(ap)^2$ in the range $2 < (ap)^2 < 3.2$. This procedure is flawed. We note that this is in danger of extrapolating perturbative errors into the infrared. In the next section we show instead how to take the continuum limit at non-zero momentum to eliminate discretisation errors. These numbers are thus for comparison only, and constitute a check and a demonstration of the precision that is possible using the techniques of this paper. The numbers do not represent an attempt to improve on previous estimates of renormalization constants for the RBC-UKQCD domain wall programme. The physical RBC-UKQCD predictions will be updated using the methods of this paper techniques in later works, where we will also use step scaling to raise the momentum scale to minimise perturbative error.



(a) $Z_m^{RI/MOM}((ap)^2) \rightarrow Z_m^{\overline{MS}}(2 \text{ GeV})$

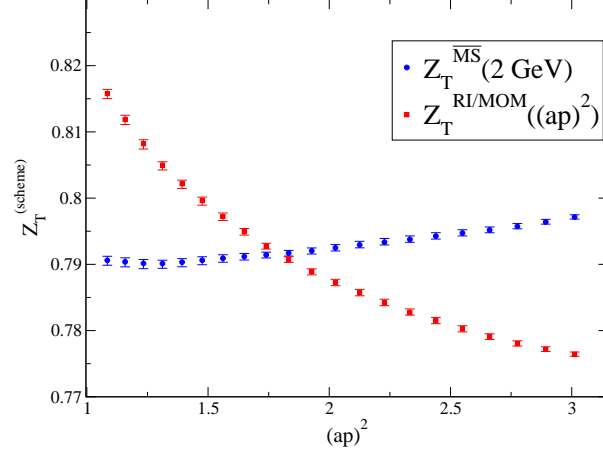


(b) $Z_m^{SMOM-\not{d}}((ap)^2) \rightarrow Z_m^{\overline{MS}}(2 \text{ GeV})$

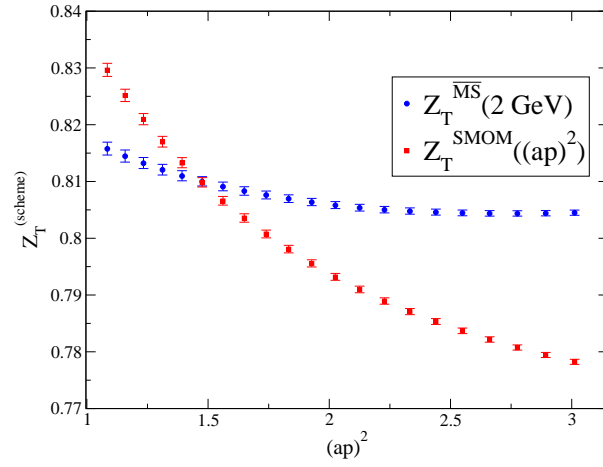


(c) $Z_m^{SMOM-\gamma_\mu}((ap)^2) \rightarrow Z_m^{\overline{MS}}(2 \text{ GeV})$

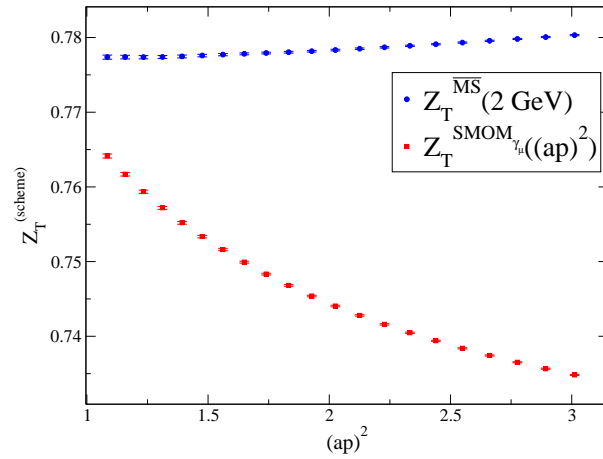
Figure 6: Z_m on the $\beta = 2.13$ lattice in a MOM scheme (red) and with the perturbative running divided out and converted to \overline{MS} (blue).



(a) $Z_T^{\text{RI/MOM}}((ap)^2) \rightarrow Z_T^{\overline{MS}}(2 \text{ GeV})$

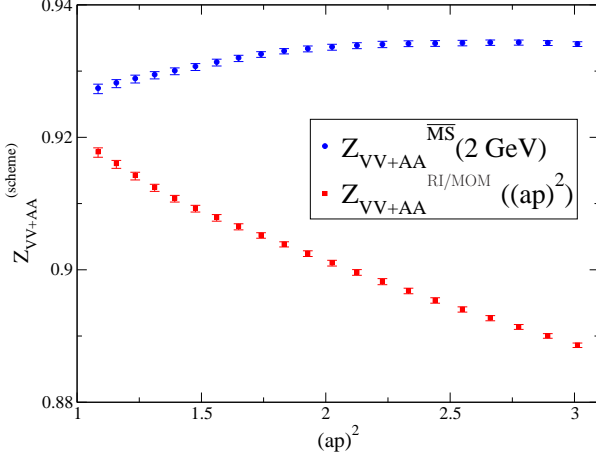


(b) $Z_T^{\text{SMOM}-\not{d}}((ap)^2) \rightarrow Z_T^{\overline{MS}}(2 \text{ GeV})$

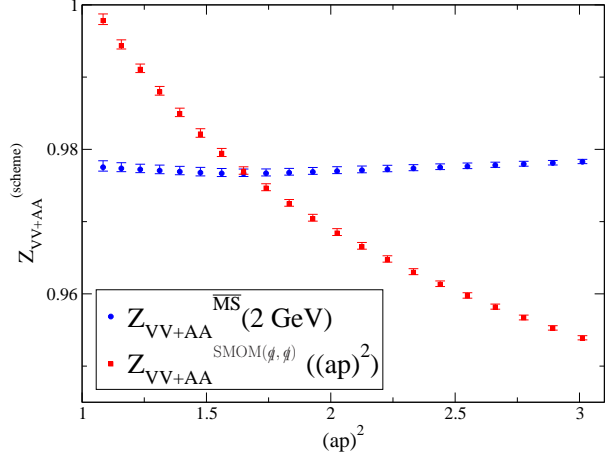


(c) $Z_T^{\text{SMOM}-\gamma_\mu}((ap)^2) \rightarrow Z_T^{\overline{MS}}(2 \text{ GeV})$

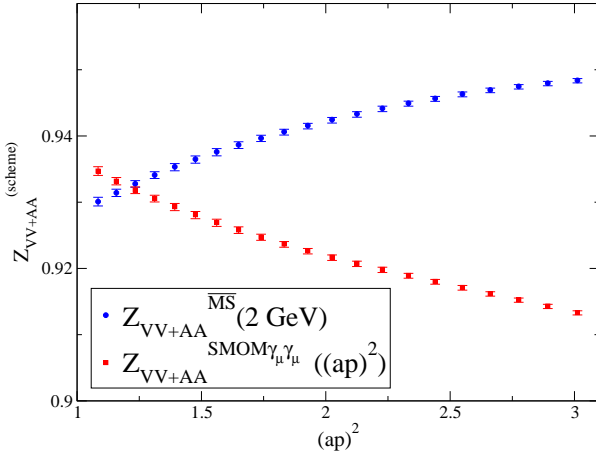
Figure 7: Z_T on the $\beta = 2.13$ lattice in a MOM scheme (red) and with the perturbative running divided out and converted to \overline{MS} (blue).



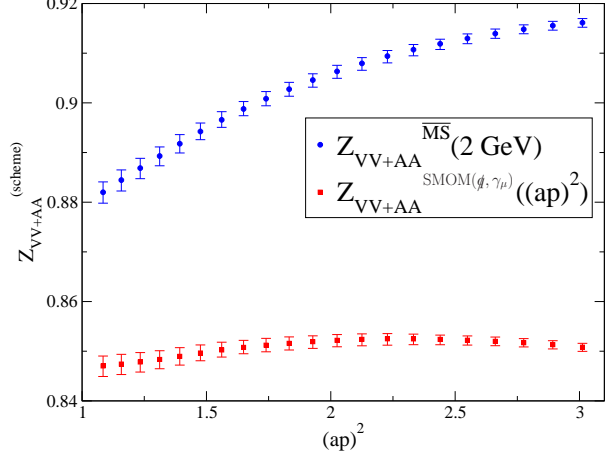
(a) $Z_{BK}^{RI/MOM}((ap)^2) \rightarrow Z_{BK}^{\overline{MS}}(2\text{GeV})$



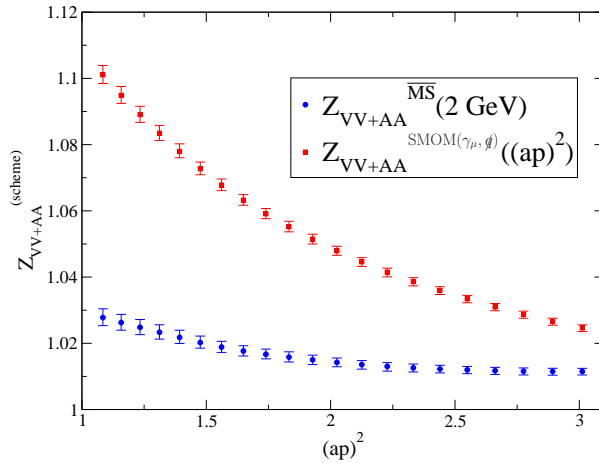
(b) $Z_{BK}^{SMOM-\not{p}-\not{p}}((ap)^2) \rightarrow Z_{BK}^{\overline{MS}}(2\text{GeV})$



(c) $Z_{BK}^{SMOM-\gamma_\mu-\gamma_\mu}((ap)^2) \rightarrow Z_{BK}^{\overline{MS}}(2\text{GeV})$



(d) $Z_{BK}^{SMOM-\not{p}-\gamma_\mu}((ap)^2) \rightarrow Z_{BK}^{\overline{MS}}(2\text{GeV})$



(e) $Z_{BK}^{SMOM-\gamma_\mu-\not{p}}((ap)^2) \rightarrow Z_{BK}^{\overline{MS}}(2\text{GeV})$

Figure 8: Z_{VV+AA} on the $\beta = 2.13$ lattice in a MOM scheme (red) and with the perturbative running divided out and converted to \overline{MS} (blue).

Z_O	Ref: [8]	RIMOM (extrap)	RIMOM	SMOM- g	SMOM- γ_μ
Z_q	0.7726(48 + 150)	0.7753(15)	0.79605(63)	0.8035(10)	0.77744(31)
Z_m	1.656(30 + 83)	1.483(28)	1.546(15)	1.5073(26)	1.5405(18)
Z_T	0.7950(34 + 150)	0.7962(13)	0.80339(62)	0.80626(73)	0.77768(20)

Table IV: The quark field, mass and tensor current renormalization constants in \overline{MS} at $2(GeV)$. Error in the first column is (stat + sys) error in the other columns statistical only. Note this work used 20 configurations at each mass whereas [8] used 300 point source measurements on 75 configurations. The third column uses the value extrapolated to zero for comparison with the results of [8]. The others use simple interpolation to obtain the value at $p^2 = 2GeV$

Ref: [8]	RIMOM (extrap)	RIMOM	SMOM- (g,g)	SMOM- (γ_μ,γ_μ)	SMOM- (g,γ_μ)	SMOM- (γ_μ,g)
0.9276(52 + 220)	0.93330(73)	0.92994(54)	0.97737(59)	0.93406(60)	1.0233(21)	0.8903(19)

Table V: BK renormalization constant with same parameters as above. The extrapolated RIMOM is for comparison with [8] the rest of the measurements use the interpolated value at $p^2 = 2GeV$.

B. Scale determination in a small volume

Determining the lattice spacing for our $\beta = 2.23$ ensemble is a useful test case for the methods of section IV B 1. As a preliminary we have calculated r_C for our 16^3 lattices. We compute timelike Wilson loops with four hits of APE smearing, smearing parameter 2.5, in the spatial direction. The tree level improvement of [35] is here required for the Iwasaki gluon action. We compute the tree level Wilson loop using code developed in [47] to obtain Table VI where the potential includes the self energy part.

$$aV(\vec{R}a) = - \lim_{T \rightarrow \infty} \frac{1}{W(\vec{R}, T)} \frac{dW(\vec{R}, T)}{dT} = C_F V(\vec{R}) g^2 + O(g^4) \quad (38)$$

By demanding

$$F(r_I) = (V(r) - V(r - a))/a = F_{tree} = \frac{1}{4\pi r_I^2} \quad (39)$$

we solve for r_I using Table VI. This approach leads to much reduced lattice $O(a^2)$ errors [35] [48]. Further, using the force instead of the potential removes the self energy part and reduces the linear term, σr , to a constant. Fitting the Cornell potential to find r_C requires σ . However, σ is dependant on the long distance behaviour of $V(r)$, and to constrain it one

\vec{R}	V_W	V_I
(1,0,0)	0.166667	0.08963(1)
(2,0,0)	0.209842	0.12569(2)
(3,0,0)	0.225186	0.13879(3)
(4,0,0)	0.232442	0.14506(4)
(5,0,0)	0.236630	0.14878(4)
(6,0,0)	0.239366	0.15133(5)
(7,0,0)	0.241300	0.15318(5)
(8,0,0)	0.242742	0.15456(5)

Table VI: V_W is the static potential tree level part with the Wilson gluon action, V_I uses the Iwasaki gluon action. As R tends to infinity the difference between successive terms for Wilson and Iwasaki actions (the force) is the same since the self energy part cancels and the two actions reproduce the same IR physics.

has to sample large r . When fitting to the force, r_C can be obtained without including large distance data in the procedure, and r_C computed this way is a finite volume safe observable with which to determine the lattice spacing.

In order to extract $V(r)$ from the average Wilson loops $\langle W(r, t) \rangle$ we first plot the effective potential

$$\log\left(\frac{\langle W(r, t+1) \rangle}{\langle W(r, t) \rangle}\right) \quad (40)$$

as a function of t . The largest value of r used in this analysis is $4a$. Excited state contamination and statistical noise are problematic, and we use the 'black box' method [49] to define an improved effective mass that takes account of the first excited state. This allows us to extend t_{min} to $t = 3$ which gives a significant error reduction compared to the usual effective mass. On the $\beta = 2.13$ lattice we use 600 configurations for each mass, each configuration rotated to use 4 different time directions. For $\beta = 2.23$ we use 750 configurations per mass and again rotate the time direction.

The equation $r^2 F(r) = C$ has solutions in the range of our data for $C \in (0.6, 2.0)$. Lower values give more accurate r_C but these are likely to have large discretisation errors. For any C however $\frac{r_C/a_{2.13}}{r_C/a_{2.23}}$ should be constant, we plot this ratio as a function of C in figure 10 and

determine $C > 1.4$ is appropriate and gives the value for the ratio of lattice scales,

$$R_a^2 = \frac{(a_{2.23})^2}{(a_{2.13})^2} = 0.652(21) \quad (41)$$

This implies a lattice spacing of $a^{-1} \simeq 2.14$ GeV for the $\beta = 2.23$ ensembles.

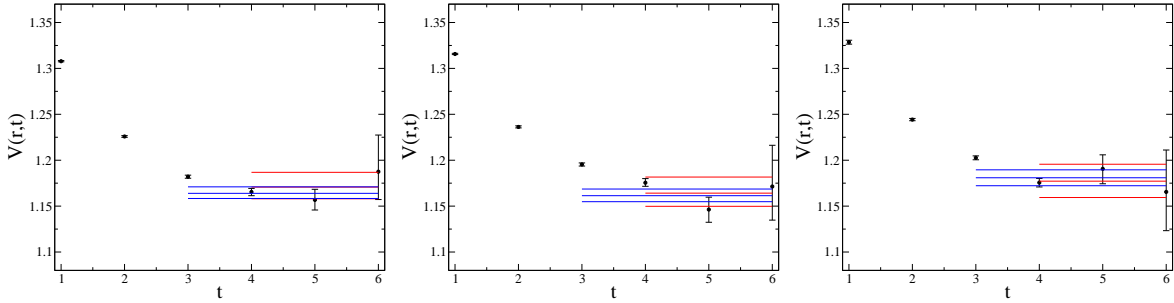


Figure 9: Effective mass plots for (left to right) $m = 0.03$, $m = 0.02$, $m = 0.01$ on the $\beta = 2.13$ lattice at $r = 4a$. Datapoints are computed via equation 40. The red constant is obtained from a fit over the last three datapoints. The blue is from the black box method with $t_{min} = 3$.

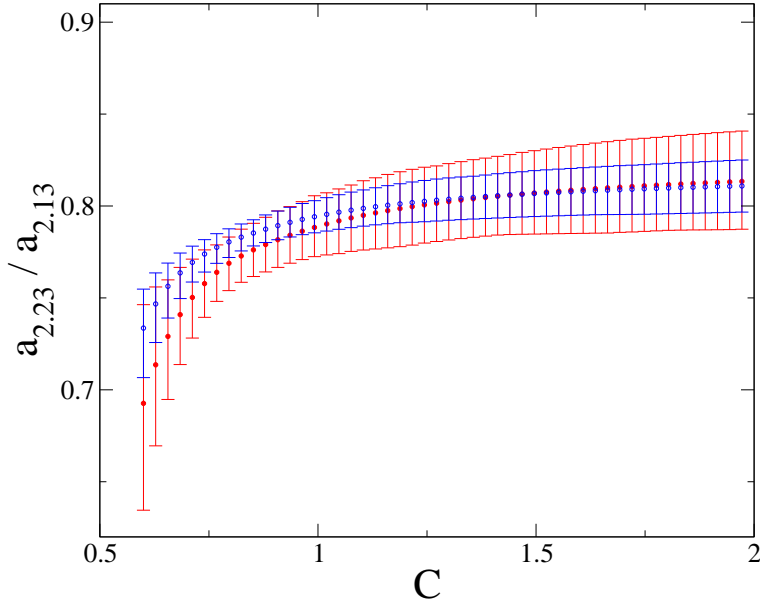


Figure 10: The ratio $\frac{r_C/a_{2.13}}{r_C/a_{2.23}}$ as a function of C . The red data is computed using the effective mass 40 $t_{min} = 4$ and the blue uses the black box method with $t_{min} = 3$, and gives the same value but with significantly smaller error.

We propose below a scale factor $s = 1.5$, and believe that at least two iterations of step scaling should be possible based only on the static potential. However, the static potential

displays percent scale errors even with many configurations and finding a more precise alternative would certainly be good in any case.

C. Continuum limit scale evolution functions

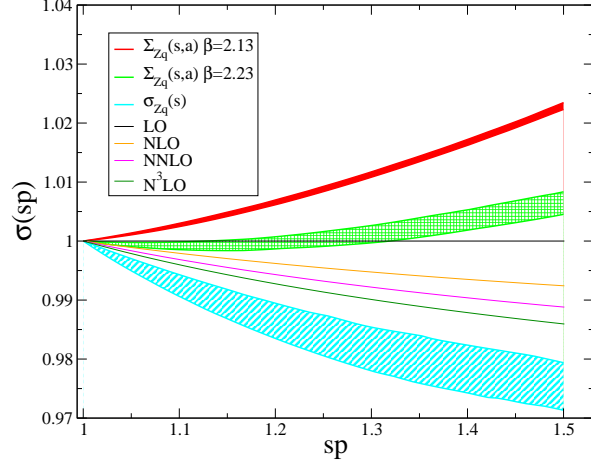
Following equation 26 we can compute $\sigma_O(p, sp)$ using two lattice spacings. We consider the evolution of renormalisation constants Z_q , Z_m , Z_T , and Z_{B_K} in both the exceptional and the non-exceptional kinematic schemes. We choose $p \simeq 2(\text{GeV})$ and compute $\sigma_O(p, sp)$ as a function of s .

Because of the very smooth p^2 dependence of the vertex functions computed with twisted boundary conditions we can perform a simple interpolation to match values of p^2 on each lattice. One could in principle simulate at the same physical momentum on each lattice by choosing the twisting angles appropriately, however since the interpolation introduced only a very small uncertainty this was not necessary.

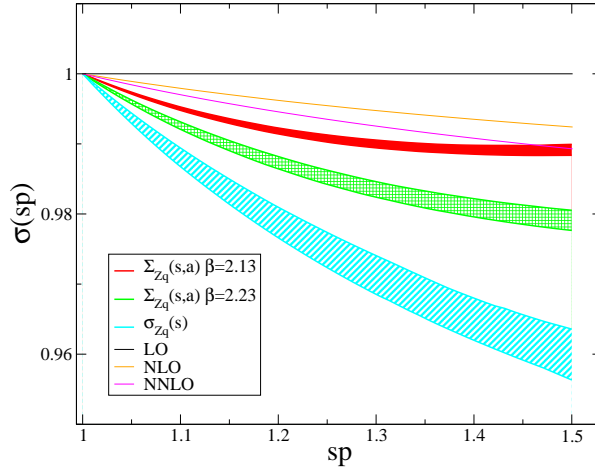
For each operator we can now evaluate $\Sigma_O(p = 2\text{GeV}, sp, a^{-1} = 1.729\text{GeV})$ and $\Sigma_O(p = 2\text{GeV}, sp, a^{-1} = 2.14\text{GeV})$. Linear extrapolation in a^2 with only two datapoints is not as robust as one might like, but certainly suffices to demonstrate the method. Using this, we can obtain the continuum limit step scaling function $\sigma_O(p = 2\text{GeV}, sp)$ for the quark field (figure 11), mass (figure 12), tensor current (figure 13), and the four quark operator \mathcal{O}_{VV+AA} (figure 14). With an appropriate third and smaller lattice spacing using a correspondingly smaller volume we could similarly determine the next step, evolving from 3 GeV to 4.5 GeV and so on.

Figure 11 is especially important, because Z_q suffers from the greatest lattice artefacts for Domain Wall Fermions, and is carefully eliminated in the NPR analysis of other operators.

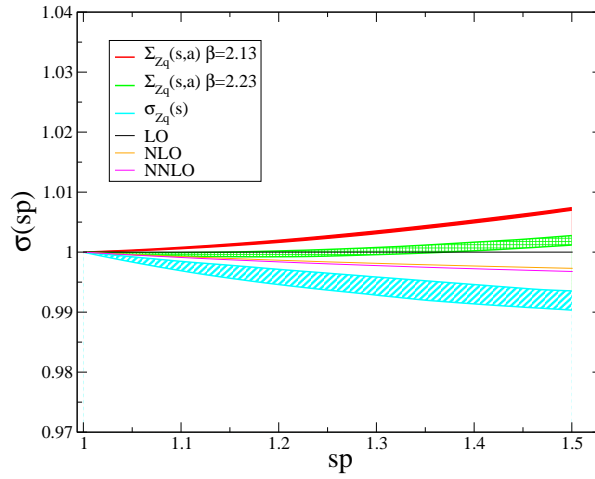
In the γ_μ scheme, with both exceptional and non-exceptional momenta, the finite lattice spacing running of Z_q is in the *opposite* direction to the perturbative prediction, however the running behaviour recovered in the continuum limit is close to perturbative. The determination of Z_q with domain wall fermions displays the momentum dependence of the exponent, $\alpha(p)$, of localisation in the fifth dimension [46]. As shown here, in a number of schemes, as long as an unambiguous continuum limit can be defined, the Domain-Wall action will then produce the continuum scaling behaviour of Z_q and the other renormalization constants.



(a) Z_q , exceptional, RI

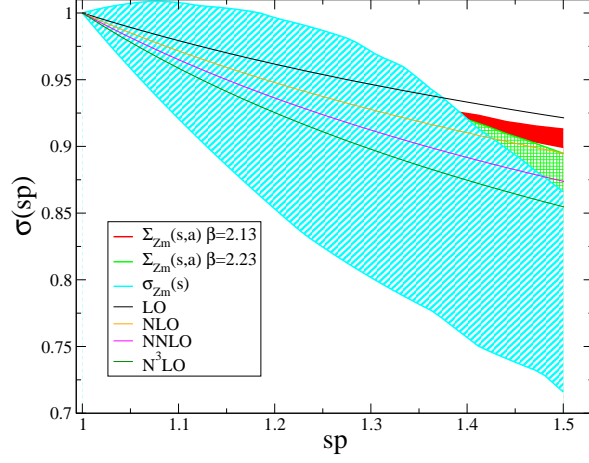


(b) Z_q , non-exceptional, $SMOM - q$

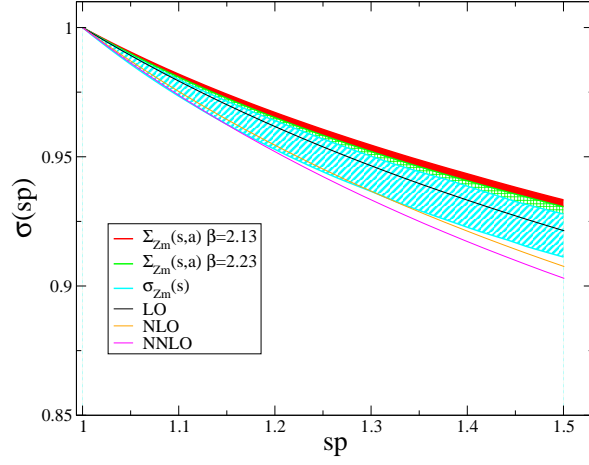


(c) Z_q , non-exceptional, $SMOM - \gamma_\mu$

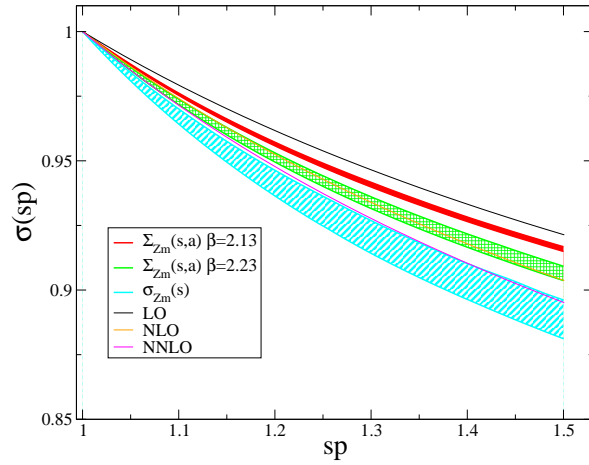
Figure 11: Quark field renormalization running from $\simeq 2$ GeV to $\simeq 3.0$ GeV in the three different schemes compared to the perturbative running in each scheme.



(a) Z_m , exceptional, RI

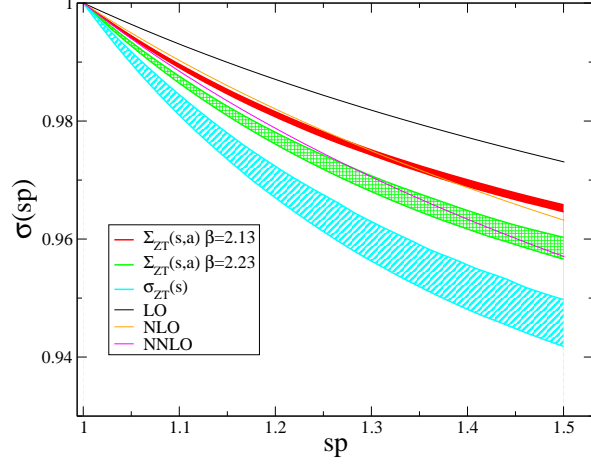


(b) Z_m , non-exceptional, $SMOM - q$

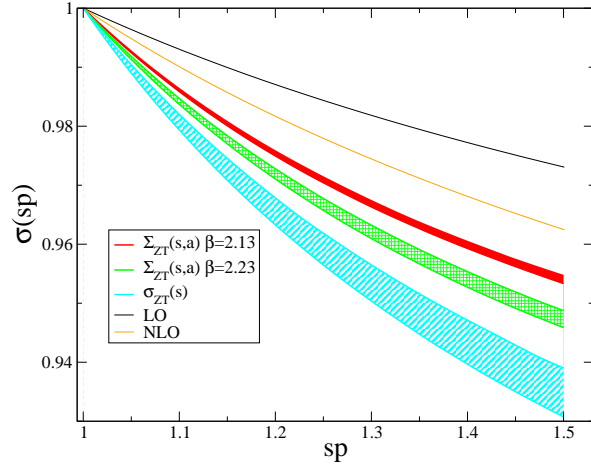


(c) Z_m , non-exceptional, $SMOM - \gamma_\mu$

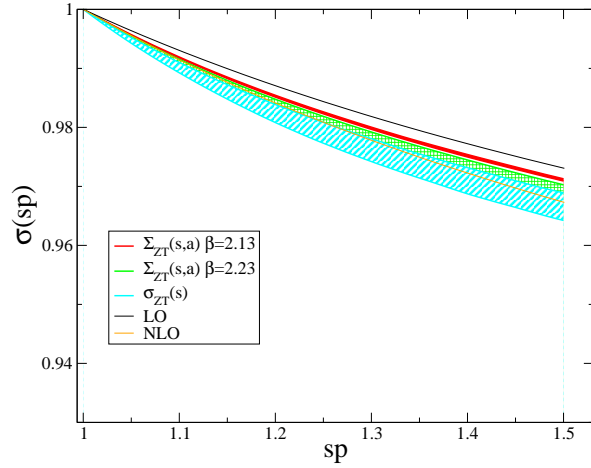
Figure 12: Quark mass renormalization running from $\simeq 2$ GeV to $\simeq 3.0$ GeV in the three different schemes compared to the perturbative running in each scheme.



(a) Z_T , exceptional, RI

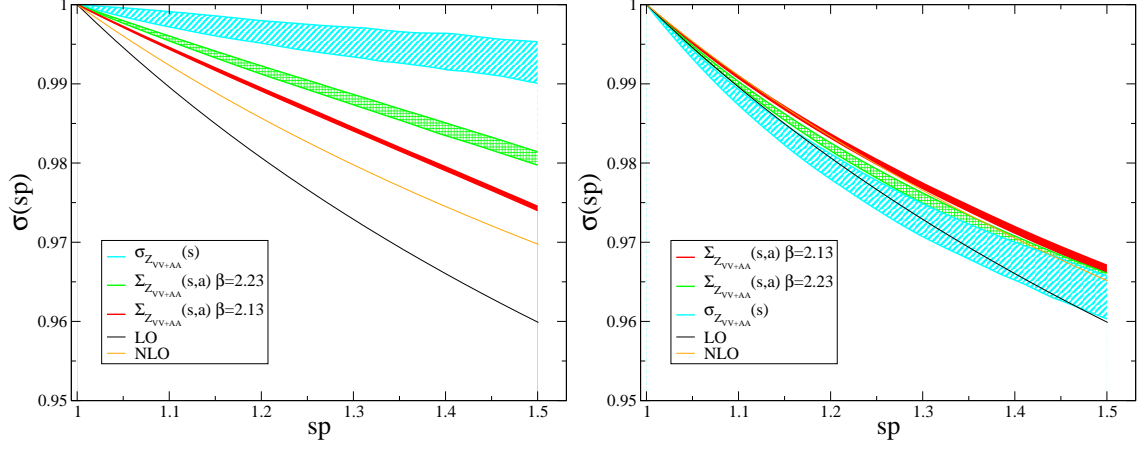


(b) Z_T , non-exceptional, $SMOM - q$



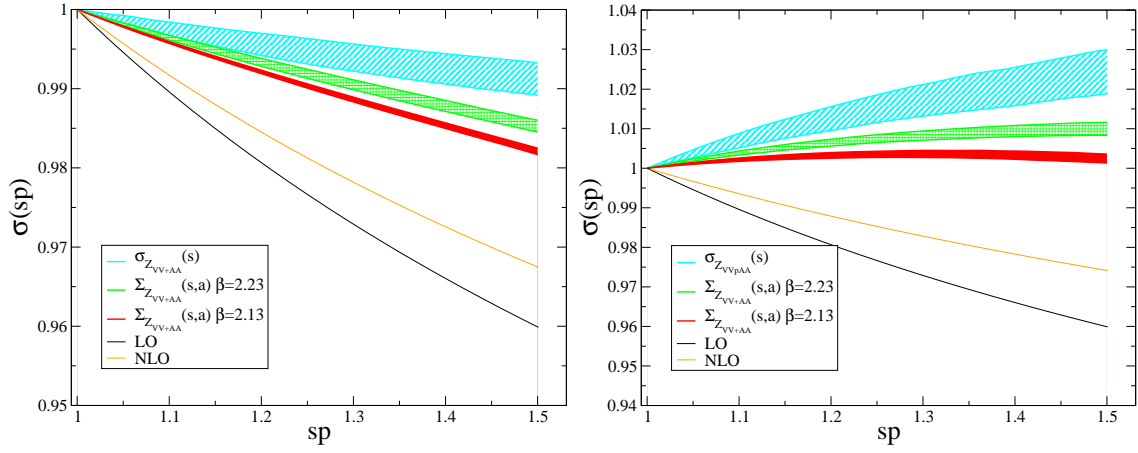
(c) Z_T , non-exceptional, $SMOM - \gamma_\mu$

Figure 13: Tensor current renormalization running from $\simeq 2$ GeV to $\simeq 3.0$ GeV in the three different schemes compared to the perturbative running in each scheme.



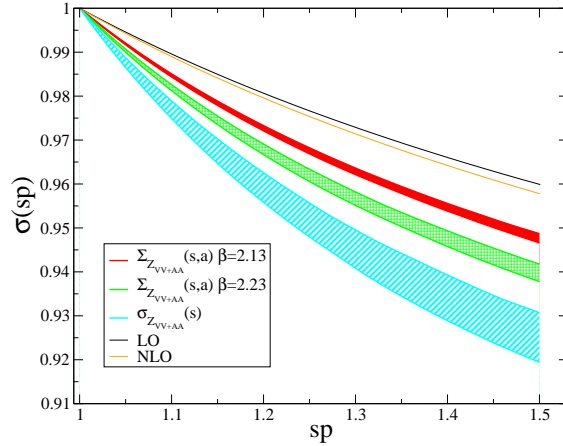
(a) Z_{BK} , exceptional, RI/MOM

(b) Z_{BK} , non-exceptional, $SMOM - (\not{p}, \not{p})$



(c) Z_{BK} , non-exceptional, $SMOM - (\gamma_\mu, \gamma_\mu)$

(d) Z_{BK} , non-exceptional, $SMOM - (\not{p}, \gamma_\mu)$



(e) Z_{BK} , non-exceptional, $SMOM - (\gamma_\mu, \not{p})$

Figure 14: Quark field renormalization running from $\simeq 2$ GeV to $\simeq 3.0$ GeV in the three different schemes compared to the perturbative running in each scheme.

VI. CONCLUSIONS

We have introduced the use of twisted boundary conditions in off-shell renormalisation. This enables controlled continuum extrapolation of the relevant amplitudes and rigorous disentangling of lattice artefacts from perturbative truncation errors in the method.

We outlined a step scaling approach based on the scheme that will allow us to raise the scales at which perturbation theory is applied. The method has been demonstrated by taking the continuum limit of the first step scaling function in the process. We can certainly raise this scale from around 2 GeV to at least around 5 GeV, and perhaps higher. The 5 GeV upper scale is limited only by the range over which our current matching based on the static potential is likely to be precise. This is, in any case, the scale above which one should consider charm and bottom quark effects. Were an appropriately precise method for matching lattice scales (or renormalised couplings) available, the method could then be applied to evolve the three flavour theory to very high momentum scales, of order M_Z .

The lattice spacing matching strategy will be the subject of further study, however, raising the scale at which, typically two or three loop, perturbation theory is applied for Rome-Southampton renormalisation for much important lattice phenomenology is already a significant step. For example, a naive estimate of an α^3 truncation error with $O(1)$ coefficient is reduced from 3% to under 1% by raising this scale to 5 GeV.

We plan to produce continuum limit scale evolution functions spanning the complete range of lattice operators covering the region 2-5 GeV. This includes all lattice bilinear and four quark operators, bilinear operators with covariant derivatives for structure functions and distribution amplitudes, and three quark operators relevant for proton decay matrix elements.

Obtaining the scaling functions in the continuum limit will enable calculations with any lattice action to raise the reference scale at which operators are quoted in \overline{MS} from 2 GeV to 5 GeV with substantial reduction in systematic errors.

VII. ACKNOWLEDGEMENTS

We would like to thank our colleagues in the RBC and UKQCD collaborations for many fruitful discussions, and particularly Yasumichi Aoki, Dirk Broemmell, Norman Christ, Taku

Izubuchi, Chris Kelly, Chris Sachrajda and Christian Sturm. We also wish to thank Luigi Del Debbio and David Lin for useful discussions. We particularly thank Chris Sachrajda and Christian Sturm for access to unpublished projectors and perturbative expressions for the SMOM schemes for the $VV + AA$ operator.

The software used includes: the CPS QCD codes http://qcdoc.phys.columbia.edu/chulwoo_index.html, supported in part by the US-DOE SciDAC program; the BAGEL [50] assembler kernel generator for many of the high-performance optimized kernels; and the UKHadron codes.

The authors were supported by PPARC grants PP/D000238/1 and PP/C503154/1. PAB acknowledges support from RCUK.

-
- [1] G. Martinelli, C. Pittori, C. T. Sachrajda, M. Testa and A. Vladikas, Nucl. Phys. B **445** (1995) 81 [arXiv:hep-lat/9411010].
 - [2] M. Gockeler *et al.*, Nucl. Phys. B **544** (1999) 699 [arXiv:hep-lat/9807044].
 - [3] V. Furman and Y. Shamir, Nucl. Phys. B **439** (1995) 54 [arXiv:hep-lat/9405004].
 - [4] Y. Iwasaki, Nucl. Phys. B **258** (1985) 141.
 - [5] T. Blum *et al.*, Phys. Rev. D **66** (2002) 014504 [arXiv:hep-lat/0102005].
 - [6] H. D. Politzer, Nucl. Phys. B **117** (1976) 397.
 - [7] P. Pascual and E. de Rafael, Z. Phys. C **12** (1982) 127.
 - [8] Y. Aoki *et al.*, Phys. Rev. D **78** (2008) 054510 [arXiv:0712.1061 [hep-lat]].
 - [9] C. Sturm, Y. Aoki, N. H. Christ, T. Izubuchi, C. T. C. Sachrajda and A. Soni, Phys. Rev. D **80** (2009) 014501 [arXiv:0901.2599 [hep-ph]].
 - [10] RBC and UKQCD collaboration “Continuum limit of B_K from 2+1 Flavor Domain Wall QCD”, in preparation.
 - [11] L. G. Almeida and C. Sturm, arXiv:1004.4613 [Unknown].
 - [12] M. Gorbahn and S. Jager, arXiv:1004.3997 [Unknown].
 - [13] Y. Aoki, “Non-perturbative renormalization in Lattice QCD”, PoS(Lattice 2009)012.
 - [14] M. Luscher, R. Sommer, P. Weisz and U. Wolff, Nucl. Phys. B **413** (1994) 481 [arXiv:hep-lat/9309005].
 - [15] M. Luscher, P. Weisz and U. Wolff, Nucl. Phys. B **359**, 221 (1991).

- [16] A. Bode *et al.* [ALPHA Collaboration], Phys. Lett. B **515** (2001) 49 [arXiv:hep-lat/0105003].
- [17] S. Sint, Nucl. Phys. B **451** (1995) 416 [arXiv:hep-lat/9504005].
- [18] S. Sint, Nucl. Phys. Proc. Suppl. **42** (1995) 835 [arXiv:hep-lat/9411063].
- [19] M. Luscher, R. Sommer, U. Wolff and P. Weisz, Nucl. Phys. B **389** (1993) 247 [arXiv:hep-lat/9207010].
- [20] M. Luscher, R. Narayanan, P. Weisz and U. Wolff, Nucl. Phys. B **384** (1992) 168 [arXiv:hep-lat/9207009].
- [21] E. Bilgici *et al.*, Phys. Rev. D **80** (2009) 034507 [arXiv:0902.3768 [hep-lat]].
- [22] Y. G. Zhestkov, PhD Thesis
- [23] Y. Zhestkov, arXiv:hep-lat/0101008.
- [24] K. Jansen *et al.*, Phys. Lett. B **372** (1996) 275 [arXiv:hep-lat/9512009].
- [25] P. A. Boyle, Nucl. Phys. Proc. Suppl. **129** (2004) 358 [arXiv:hep-lat/0309100].
- [26] P. F. Bedaque, Phys. Lett. B **593** (2004) 82 [arXiv:nucl-th/0402051].
- [27] G. M. de Divitiis, R. Petronzio and N. Tantalo, Phys. Lett. B **595** (2004) 408 [arXiv:hep-lat/0405002].
- [28] C. T. Sachrajda and G. Villadoro, Phys. Lett. B **609** (2005) 73 [arXiv:hep-lat/0411033].
- [29] J. M. Flynn, A. Juttner and C. T. Sachrajda [UKQCD Collaboration], Phys. Lett. B **632** (2006) 313 [arXiv:hep-lat/0506016].
- [30] P. A. Boyle, J. M. Flynn, A. Juttner, C. T. Sachrajda and J. M. Zanotti, JHEP **0705** (2007) 016 [arXiv:hep-lat/0703005].
- [31] P. A. Boyle *et al.*, Phys. Rev. Lett. **100** (2008) 141601 [arXiv:0710.5136 [hep-lat]].
- [32] D. J. Antonio *et al.*, arXiv:hep-lat/0702026.
- [33] P. A. Boyle *et al.*, JHEP **0807** (2008) 112 [arXiv:0804.3971 [hep-lat]].
- [34] P. A. Boyle *et al.*, arXiv:1004.0886 [Unknown].
- [35] S. Necco and R. Sommer, Nucl. Phys. B **622** (2002) 328 [arXiv:hep-lat/0108008].
- [36] R. Sommer, Nucl. Phys. B **411** (1994) 839 [arXiv:hep-lat/9310022].
- [37] C. Allton *et al.* [RBC and UKQCD Collaborations], Phys. Rev. D **76** (2007) 014504 [arXiv:hep-lat/0701013].
- [38] D. J. Antonio *et al.* [RBC and UKQCD Collaborations], Phys. Rev. D **75** (2007) 114501 [arXiv:hep-lat/0612005].
- [39] D. J. Antonio *et al.* [RBC Collaboration and UKQCD Collaboration], Phys. Rev. D **77** (2008)

- 014509 [arXiv:0705.2340 [hep-lat]].
- [40] RBC-UKQCD Collaboration, “Continuum Limit Physics from 2+1 Flavor Domain Wall QCD”
In preparation
- [41] C. Allton *et al.* [RBC-UKQCD Collaboration], Phys. Rev. D **78** (2008) 114509
[arXiv:0804.0473 [hep-lat]].
- [42] K. G. Chetyrkin and A. Retey, Nucl. Phys. B **583**, 3 (2000) [arXiv:hep-ph/9910332].
- [43] J. A. Gracey, Nucl. Phys. B **662** (2003) 247 [arXiv:hep-ph/0304113].
- [44] A. J. Buras, M. Misiak and J. Urban, Nucl. Phys. B **586** (2000) 397 [arXiv:hep-ph/0005183].
- [45] M. Ciuchini, E. Franco, V. Lubicz, G. Martinelli, I. Scimemi and L. Silvestrini, Nucl. Phys. B
523 (1998) 501 [arXiv:hep-ph/9711402].
- [46] Y. Shamir, Nucl. Phys. B **406** (1993) 90 [arXiv:hep-lat/9303005].
- [47] G. S. Bali and P. Boyle, arXiv:hep-lat/0210033.
- [48] A. Hasenfratz, R. Hoffmann and F. Knechtli, Nucl. Phys. Proc. Suppl. **106** (2002) 418
[arXiv:hep-lat/0110168].
- [49] G. T. Fleming, arXiv:hep-lat/0403023.
- [50] P. A. Boyle, “The BAGEL assembler generator”, Computer Physics Communications
180/12:2739 (2009) [doi:10.1016/j.cpc.2009.08.010]